



ELSEVIER

Ultramicroscopy 61 (1995) 99–104

---

---

ultramicroscopy

---

---

## “Tunnel” near-field optical microscopy: TNOM-2

B. Hecht <sup>a,\*</sup>, D.W. Pohl <sup>a</sup>, H. Heinzelmann <sup>b</sup>, L. Novotny <sup>c</sup>

<sup>a</sup> IBM Research Division, Zurich Research Laboratory, CH-8803 Rüschlikon, Switzerland

<sup>b</sup> Institut für Physik, Universität Basel, CH-4056 Basel, Switzerland

<sup>c</sup> Institut für Feldtheorie und Höchstfrequenztechnik, ETH Zürich, CH-8092 Zurich, Switzerland

Received 9 May 1995; accepted 11 May 1995

---

### Abstract

Light emitted from the aperture of a near-field optical probe in the close vicinity of a dielectric object propagates in classically “forbidden” as well as “allowed” directions; the two zones are separated by the critical angle for total internal reflection. The new “tunnel” near-field optical microscopy (TNOM) technique makes use of forbidden and allowed radiation, in contrast to *standard* scanning near-field optical microscopy (SNOM or NSOM), which records only the allowed light. Scan images obtained with allowed and forbidden light are complementary to some extent; the latter, however, provide high contrast and resolution even in situations in which standard SNOM/NSOM shows little or no contrast. The influence of topography on image formation is analyzed and discussed.

---

### 1. Introduction: TNOM concept

The “tunnel” *near-field optical microscope* (TNOM) [1], which might also be called forbidden-light scanning near-field optical microscope (SNOM or NSOM), detects not only regularly transmitted light but also radiation coupled via evanescent waves, i.e. photon tunneling, into an object. This radiation propagates into the sample and its substrate in classically forbidden directions, i.e. at angles larger than the critical angle for total internal reflection (TIR).

Like standard aperture SNOM, TNOM employs an aperture optical probe, which defines a very small interaction volume [2,3]. In its operating principle, TNOM also resembles the (photon) scanning tunneling optical microscope (STOM, also called PSTM

[4–6]): The evanescent wavelets emerging from a subwavelength-sized aperture excite TIR-type, laterally extended evanescent waves at the substrate surface (i) directly and (ii) indirectly via coupling to localized evanescent waves characteristic for the object structures. Both contributions require freely propagating waves into the forbidden regime in order to satisfy the boundary conditions, but only the second contains the small-scale object information of interest. Our experimental and theoretical results indicate that the evanescent wave/evanescent wave interaction (ii) is very sensitive to small variations of the sample surface.

### 2. TNOM-2 setup

For practical applications it is important to collect as much transmitted light as possible. Having attained some understanding of the principles of for-

---

\* Corresponding author.

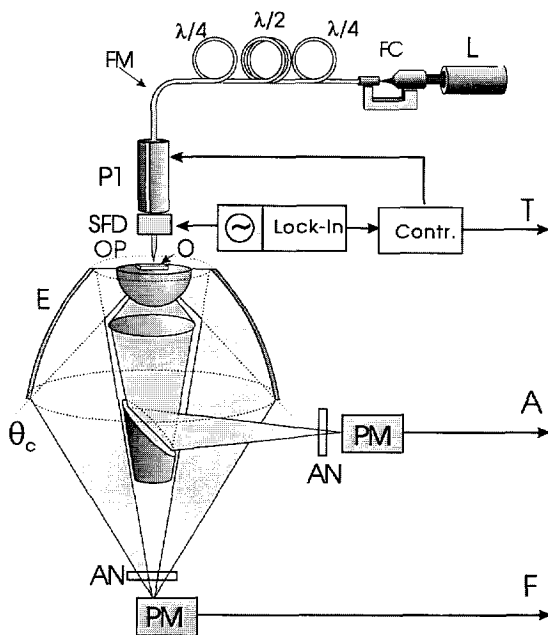


Fig. 1. TNOM-2 setup for global detection: (L) laser; ( $\lambda/2$ ,  $\lambda/4$ ) combination of  $\lambda/2$  and  $\lambda/4$  plates for polarization adjustment; (FC) fiber coupler; (FM) monomode fiber with pointed end acting as optical probe (OP); (P1) piezoactuator; (SFD) shear force detector; (E) elliptical mirror; ( $\theta_c$ ) critical angle; (O) object; (AN) polarization analyzers; (PM) photomultipliers detecting allowed (A) and forbidden (F) light. Channel T provides the topographic signal derived from the frictional (shear) force interaction. From Ref. [7], reprinted by permission of Kluwer Academic Publishers.

bidden-light imaging, we replaced the optical fiber cables used in TNOM-1 [1] as receivers of the transmitted radiation by an *elliptical mirror* for the forbidden radiation, and by an objective lens for

allowed radiation. The new arrangement, called TNOM-2 [7], is shown in Fig. 1.

The illumination part is that of a standard SNOM [2,3] with metal-coated fiber tips having an aperture of 50–80 nm at the apex. The shear force detection (SFD) method [8,9] was applied in combination with a miniaturized fiber interferometer [7]. The amplitude of oscillation can be kept as small as 1 nm ptp, which has the following advantages:

- \* very stable feedback operation,
- \* improved tip lifetime (lower energy dissipation?),
- \* improved resolution.

In order to detect allowed as well as forbidden transmitted radiation simultaneously, total reflection at the exit face of the sample substrate has to be avoided. We therefore employ a hemispherically shaped substrate in the present setup (see Fig. 1). In combination with the elliptical mirror (forbidden light) and the objective (allowed light), the collection efficiency equals that of a microscope objective with a numerical aperture of  $N.A. = 1.51$ . The TNOM-2 arrangement can, however, admit thick samples, in contrast to high-N.A. objectives.

### 3. Results

#### 3.1. Phase objects

##### 3.1.1. Experimental findings

We first studied a very simple object structure (Fig. 2): a bare glass grating with a period of 383 nm and a step height of 8 nm. Its elevations and valleys

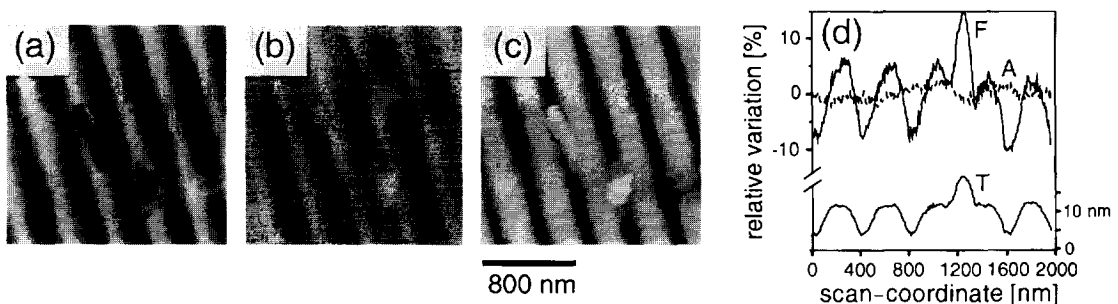


Fig. 2. Images of a bare glass grating with period 383 nm, step height 8 nm (prepared by B. Curtis, PSI Zurich), polarization perpendicular to grating lines: (a) forbidden light; (b) allowed light; (c) topography (friction image); (d) scan lines through the center of the major perturbation seen in (a)–(c). (A) allowed, (F) forbidden light; (T) topography. Adapted from Ref. [7].

are of equal width [7]. The elevations (depressions) are distinctly wider (190 nm) than the aperture diameter (50 nm), but still small compared to the wavelength (514 nm). If the SNOM signal depended only on the properties of the immediate proximity of the aperture, no difference between the “top” and “bottom” positions indicated in the figure should exist; only the steps ought to appear in a SNOM image. The images shown in Fig. 2, in agreement with the results of various related studies [1,7,10,11], however, indicate that stripes 100 to 200 nm in width are indeed visible in SNOM images, bearing an obvious similarity to the topographic structure (Fig. 2) [7]. To understand this result, one might think of a number of mechanisms:

- (1) The glass in the surface layer of a valley might differ from the material of the elevation due to the manufacturing process.
- (2) The gap width is larger when the tip is above a valley because it cannot penetrate it completely.
- (3) Elevations and valleys may be considered to a first approximation as being convex and concave parts of the surface, respectively. These opposite curvatures may influence the spreading and propagation of the transmitted radiation.

Careful inspection of the topography recorded by means of SFD as well as with a standard AFM,

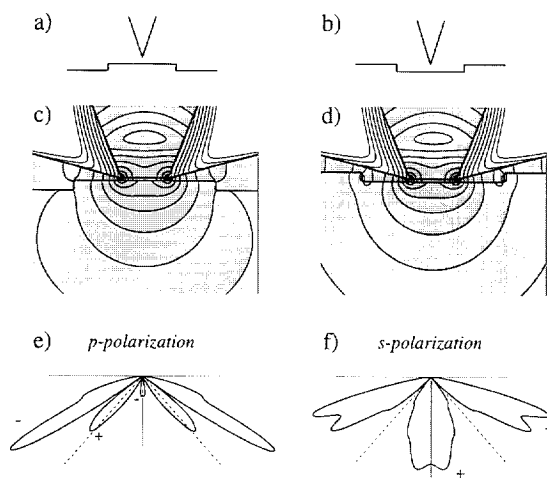


Fig. 3. SNOM probe scanning a glass grating: Are (a) “top” and (b) “valley” positions optically equivalent? (c, d) Computed electrical energy distributions, 2D model. p-polarization [7]. (e, f) Radiation patterns, difference between top and bottom positions. From Ref. [20].

Table 1

Contrast of elevations and depressions of a glass grating; comparison between 2D model SNOM and experiment [7] (from Ref. [20])

Contrast [%]	Calculated s-polarization	Calculated p-polarization	Experiment p-polarization
Allowed	1.6	3.4	4
Forbidden	-5.6	-10.1	-12

however, gave no evidence of increased roughness in the valleys. We therefore believe that differences in surface structure are insignificant, in agreement with the manufacturer [12]. Comparison with the experimentally observed contrast further rules out the second hypothesis because the valleys are brighter than the elevations in forbidden light, opposite to what one would expect on the basis of approach curves. The observed behavior, however, is in agreement with hypothesis (3) insofar as the laws of classical optics would predict a focusing effect for the convex elevation, i.e. a concentration of radiation in the forward direction, and the opposite for the concave valley.

### 3.1.2. Theoretical considerations

To substantiate this assumption, the influence of surface “curvature” was studied numerically, simulating the electromagnetic fields in the geometries sketched in Figs. 3a and 3b. Computations were restricted to the two-dimensional model SNOM introduced previously [13] because the resulting field distributions strongly resemble those of the corresponding three-dimensional configuration [14].

Figs. 3c and 3d depict the computed near fields for p- (TM-) polarization (with regard to stripe orientation) for “top” and “valley” positions of the optical probe. One clearly sees the focusing/defocusing effects of the two topographies. A similar but smaller variation exists for the near fields of s- (TE-) polarized light. The differences between the radiation patterns of top and bottom positions are plotted in Figs. 3e and 3f for p- and s-polarization. For both polarizations, the side lobes, which represent the forbidden radiation, are negative, meaning that elevations indeed appear darker than depressions. The opposite is true for the forward lobes, which represent the allowed light. The calculated contrast is compared in Table 1 with experimental

values from Fig. 2. The direction of observation was in the plane of polarization, almost perpendicular to the direction of the stripes, corresponding to p-polarization. The contrast is defined as  $2(\Phi_{\text{top}} - \Phi_{\text{valley}})/(\Phi_{\text{top}} + \Phi_{\text{valley}})$ . The agreement both with regard to the sign and to the improved contrast of the forbidden image is remarkable. The close proximity of the numerical values is considered to be coincidental. The results of Fig. 3 further suggest a reversal of contrast for forbidden and allowed light for small phase objects. Such contrast reversal is indeed found for the small “dust particles” also seen in Fig. 2.

### 3.2. Amplitude objects

#### 3.2.1. Metal island film

The second test object was a metal island film structured by means of the latex sphere shadowing

method [15]. The metal islands (Al, thickness 15 nm) were deposited at the interstices between a (later removed) array of close-packed 220 nm diameter latex balls. They form a hexagonal pattern of nearly triangular patches approximately 50 nm in width (Fig. 4b, inset). Having a penetration depth of 6 nm at  $\lambda = 515$  nm, the residual transmission of the patches, calculated in the classical manner, is about 8%. The sample can hence be used as an amplitude test object. Viewed with a conventional optical microscope (Zeiss Axioplan, objective  $50\times$ , N.A. = 0.75) it was not possible to recognize the structure.

Figs. 4a–4c depict top views of the simultaneously recorded forbidden, allowed and friction/topographic images of the metal island film (brightness equals signal level, a natural representation of the optical image). The metal islands appear as dark patches in Fig. 4a, whereas they are barely visible in Fig. 4b. In Fig. 4c, they appear bright, being eleva-

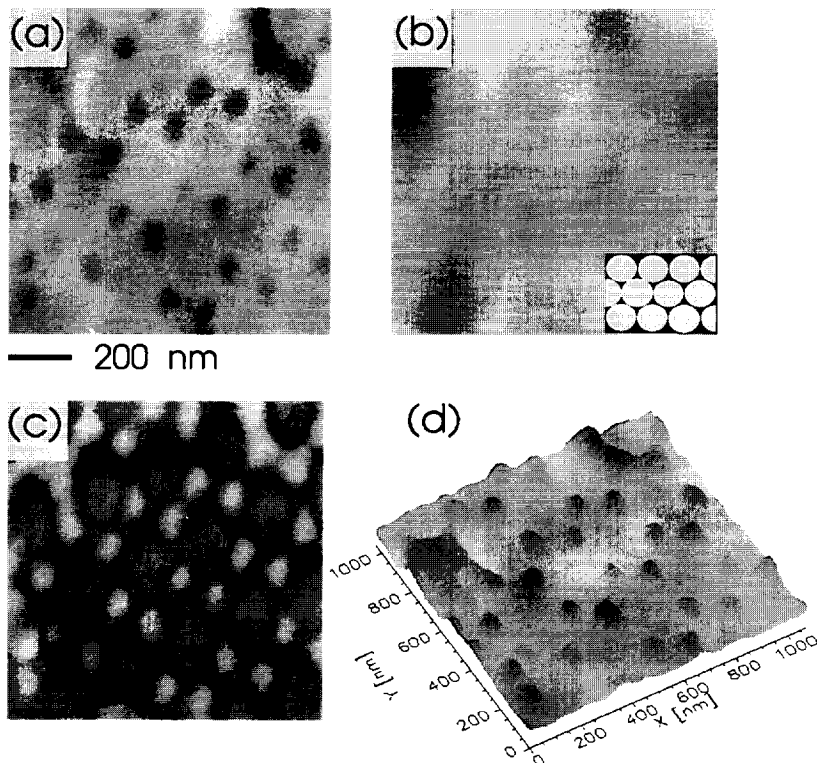


Fig. 4. Metal island film (latex sphere shadow mask): Al, thickness 15 nm, lateral extension of the metal islands: approximately 50 nm, prepared by U.Ch. Fischer, University of Münster. (a) Forbidden light, (b) allowed light, (c) topography (friction), (d) superposition of (a) and (c) highlighting the close correlation between topography and optical transmission. From Ref. [7], reprinted by permission of Kluwer Academic Publishers.

tions. The hexagonal symmetry can be clearly recognized, as well as some of the frequent lattice defects, which make the sample particularly suitable as a test object. Even the nearly triangular shape of the patches is reproduced in some cases. Fig. 4d is a superposition of Figs. 4a and 4c.

The allowed image (Fig. 4b) was probably corrupted by a stray light effect. In fact, the fiber probes used in this series of measurements had fairly large pinholes at the shank, a manufacturing problem at the time the picture was taken. On the basis of previous results with amplitude objects, cf. for instance Ref. [16], and computer simulations [13], the “interstices” should also appear dark in the allowed images.

### 3.2.2. IBM logo

The third test object (Fig. 5) shows an artistic version of IBM’s logo (I = eye, B = bee) implemented by lithographic techniques as a 5 nm titanium plus 5 nm gold semitransparent layer on glass. In this case the structure appears dark in both the

forbidden and the allowed image, identifying it as an amplitude object.

## 4. Conclusions

The results obtained from the grating test structure suggest that the recorded light flux does not depend on the *local* optical properties of the object alone but also on the environment within a distance of several aperture diameters. A number of previous theoretical investigations actually arrived at similar results, see for instance [17,18]; these studies, however, did not allow direct comparison with our experimental results because the models used differed significantly from the present TNOM setup.

Non-local effects are also known to have an influence on images obtained with scanning tunneling microscopy and AFM. The “interference patterns” recorded in Eigler et al.’s famous *quantum corral* experiment [19], for instance, fall into this category, as do the difficulties of imaging soft tissues with AFM. In both cases it is still possible to recog-

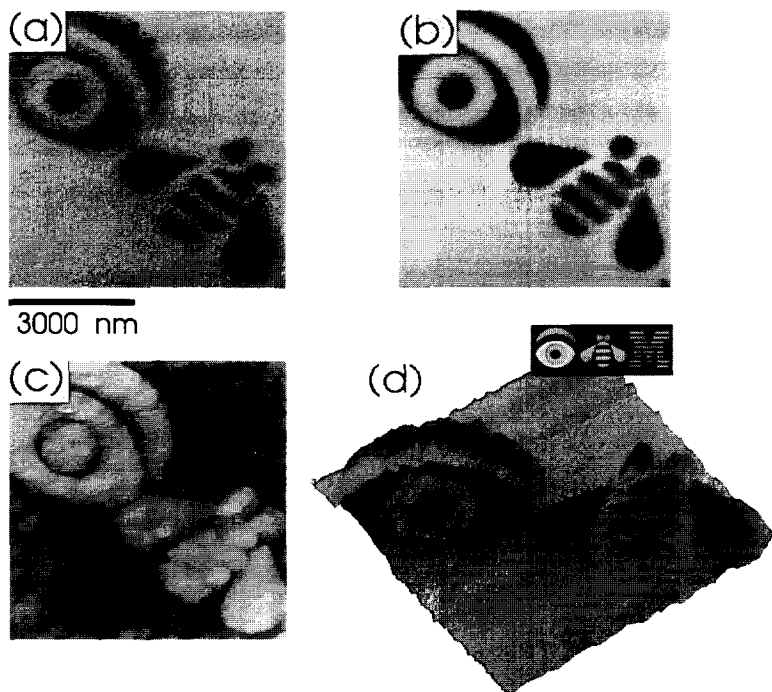


Fig. 5. Lithographic “eye-bee-(M)” logo, 5 nm Ti + 5 nm Au, seen with (a) forbidden, (b) allowed light, (c) with the “shear force” detector; (d) superposition of (a) and (c). From Ref. [20].

nize very small structures, the signatures of which are superimposed on longer-range structures. This is obviously also the case in the present near-field optical investigation.

The results of our investigations further suggest that very small phase objects appear with reverse contrast in allowed and forbidden light images, while *amplitude objects* cause negative contrast in both types of images. *Forbidden light* images combined with *allowed light* images hence allow one to distinguish between amplitude and phase, which is instrumental for quantitative image interpretation.

## 5. Summary

- \* A *sizable portion* of the light transmitted by the optical probe into the object flows in the *forbidden* directions.
- \* SNOM images represent a superposition of strictly local and non-local contributions from the near-field range.
- \* Images obtained with forbidden light provide high contrast and are insensitive to stray light.
- \* Small phase objects can be distinguished from amplitude objects by comparing forbidden and allowed images.

## Acknowledgements

The authors are grateful to B. Curtis and U.Ch. Fischer, who provided the glass grating and the latex sphere shadow mask, respectively. This work was supported in part by a grant from the priority program OPTIQUE of the Board of the Swiss Federal Institutes of Technology.

## References

- [1] B. Hecht, H. Heinzelmann and D.W. Pohl, Ultramicroscopy 57 (1995) 228.
- [2] D.W. Pohl, W. Denk and M. Lanz, Appl. Phys. Lett. 44 (1984) 651.
- [3] E. Betzig and J. Trautman, Science 257 (1992) 189.
- [4] D. Courjon, K. Sarayeddine and M. Spajer, Opt. Commun. 71 (1989) 23.
- [5] F. de Fornel, J.P. Goudonnet, L. Salomon and E. Lesniewska, Proc. SPIE 1139 (1994) 2927.
- [6] R.C. Reddick, R.J. Warmack and T.L. Ferrell, Phys. Rev. B 39 (1989) 767.
- [7] B. Hecht, D.W. Pohl, H. Heinzelmann and L. Novotny, "Tunnel" near-field optical microscopy: TNOM-2, in: Photons and Local Probes, Eds. O. Marti and R. Möller, NATO ASI Ser. E: Applied Sciences (Kluwer, Dordrecht, in preparation).
- [8] R. Toledo-Crow, P.C. Yang, Y. Chen and M. Vaez-Iravani, Appl. Phys. Lett. 60 (1992) 2957.
- [9] E. Betzig, P.L. Finn and S.J. Weiner, Appl. Phys. Lett. 60 (1992) 2484.
- [10] C. Bainier, S. Leblanc and D. Courjon, in: Near Field Optics, Eds. D.W. Pohl and D. Courjon, NATO ASI Ser. E: Applied Sciences, Vol. 242 (Kluwer, Dordrecht, 1993) p. 97.
- [11] F. de Fornel, E. Bourillot, P. Adam, L. Salomon, G. Chabrier and J.P. Goudonnet, in: Near Field Optics, Eds. D.W. Pohl and D. Courjon, NATO ASI Ser. E: Applied Sciences, Vol. 242 (Kluwer, Dordrecht, 1993) p. 59.
- [12] B. Curtis, Paul Scherrer Institute, Zurich, private communication.
- [13] L. Novotny, D.W. Pohl and P. Regli, J. Opt. Soc. Am. A 11 (1994) 1768.
- [14] L. Novotny and D.W. Pohl, Light propagation in scanning near-field optical microscopy, in: Photons and Local Probes, Eds. O. Marti and R. Möller, NATO ASI Ser. E: Applied Sciences (Kluwer, Dordrecht, in preparation).
- [15] U.Ch. Fischer and H.P. Zingsheim, J. Vac. Sci. Technol. 19 (1981) 881.
- [16] U. Dürig, D.W. Pohl and F. Rohner, J. Appl. Phys. 59 (1986) 3318.
- [17] D. Van Labeke and D. Barchiesi, J. Opt. Soc. Am. A 9 (1992) 732.
- [18] N. Garcia, A direct solution to the inverse scattering problem in near-field optical microscopy: object structure reconstruction (preprint).
- [19] E.J. Heller, M.F. Crommie, C.P. Lutz and D.M. Eigler, Nature 369 (1994) 4646.
- [20] D.W. Pohl, L. Novotny, B. Hecht and H. Heinzelmann, Radiation coupling and image formation in scanning near-field optical microscopy, in: Proc. Int. Symp. on Ultra Materials for Picotransfer, Chiba, Japan, March 1995 [in: Thin Solid Films, to be published].